Proceedings of the 1996 IEEE/SICE/RSJ International Conference on Multisensor Fusion and Integration for Intelligent Systems

Evidential Logical Sensing using Multiple Sonars for the Identification of Target Primitives in a Mobile Robot's Environment *

Birsel Ayrulu[1], Billur Barshan[1], İsmet Erkmen[2]and Aydan Erkmen[2]

[1]Department of Electrical Engineering
Bilkent University
Bilkent, 06533 Ankara, Turkey

[2]Department of Electrical Engineering
Midle East Technical University
06531 Ankara, Turkey

Abstract

Physical models are used to model reflections from target primitives commonly encountered in mobile robot applications. These targets are differentiated by employing a multi-transducer pulse/echo system which relies on both amplitude and time-of-flight (TOF) data in the feature fusion process, allowing more robust differentiation. Target features are generated as being evidentially tied to degrees of belief which are subsequently fused for multiple logical sonars at different geographical sites. This evidential approach helps to overcome the vulnerability of echo amplitude to noise and enables the modeling of non-parametric uncertainty. Feature data from multiple logical sensors are fused with Dempster-Shafer rule of combination to improve the performance of classification by reducing perception uncertainty. Using three sensing nodes, improvement in differentiation is between $20-40\%$ *without false decision, at the cost of additional computation. Simulation results are verified by experiments with a real sonar system. This evidential approach helps to overcome the vulnerability of the echo amplitude to noise and enables the modeling of non-parametric uncertainty in real time.*

1 Introduction

Sensorimotor information processing in mobile robots requires the handling of a multitude of information obtained from robot subprocesses of different types, resolution and uncertainties, such as mechanical, sensory and control subsystems. The high variety of representations, accuracy and refinement involved in sensorimotor control of mobile robots in unstructured and crowded environments renders in turn, the information space extremely ill structured where some processes may be deterministic while others are stochastic and even possibilistic in nature.

More specifically, target recognition in mobile robots on sensorimotor information processing involves reasoning, learning and acting under multisensor data which are generally incomplete, imprecise and possibly inconsistent. Furthermore, it also requires the decision making in such unstructured and dynamic environments to be reliable and robust to data failures, uncertainty, partial information, and be flexible by being adaptable to changes in the environmental data acquisition.

The objective in this paper is to fuse information from uncertain environmental data acquired by moving sonars for the strategic target recognition in the sensorimotor control of a mobile robot.

One mode of sensing which is potentially very useful and cost-effective for mobile robot applications is sonar. Since acoustic sensors are light, robust and inexpensive devices, they are widely used in mobile robot applications [1, 2, 3, 4, 5]. The most popular sonar ranging system is based on *time-of-flight* (TOF) measurement which is the time elapsed between the transmission of a pulse and its reception [6]. For improved target classification, multi-transducer pulse/echo systems which rely on *both* amplitude and TOF information can be employed. In earlier work by Barshan and Kuc, a methodology based on TOF and amplitude information is introduced to differentiate planes and corners [7]. Here, we extend this work and fuse the decisions of multiple sensing agents at distinct geographical sites using a belief function approach. The ultrasonic reflection process from commonly encountered target primitives is modeled such that sonar pairs became evidential logical sensors. Logical sensors as opposed to physical sensors that acquire actual data, *process* real sensory data in order to generate perception units which are context-dependent interpretations of actual data. An automated perception system for mobile robots fusing uncertain sensory information must be reliable in the sense that it is predictable. Therefore quantitative approaches to uncertainty are needed. These considerations favor measure-based methods handling sensory data (both physical and

*This research is supported by TÜBİTAK under grants EEEAG-92 and EEEAG-116.

0-7803-3700-X/96 $5.00

logical) at different levels of granularity related to the resolution of the data as well as the time constants of the different sensors. This desire motivates our attempt to abstract the sensor integration problem in a conceptual model where uncertainty about evidence and knowledge can be measured and systematically reduced.

Section 2 explains the sensing configuration used in this study and introduces the target primitives. In Section 3, beliefs are assigned to these target primitives based on both TOF and amplitude characteristics of the data. A description of feature fusion is included when multiple sensing sites are used. Consensus of multiple sensors at these sites is obtained by using the Dempster-Shafer rule of combination. Simulation results are provided in Section 4. In Section 5, the methodology is verified experimentally in an uncluttered rectangular room where the feature fusion process is demonstrated by employing one to three sensing sites. In the last section, concluding remarks are made and directions for future research are motivated.

2 Sonar Sensing

The most popular sonar ranging system is the TOF system. In this system, an echo is produced when the transmitted pulse encounters an object and a range value r is produced when the echo amplitude waveform first exceeds a preset threshold level τ:

$$r = \frac{ct_o}{2} \tag{1}$$

Here t_o is the TOF of the echo signal at which the echo amplitude first exceeds the threshold level and c is the speed of sound in air ($c = 343.3$ m/s at room temperature).

In this study, the far-field model of a piston type transducer having a circular aperture is used [8]. The amplitude of the echo decreases with the inclination angle θ, which is the deviation angle from normal incidence as illustrated in Figure 1. The echo amplitude falls below the threshold level when the inclination angle θ is greater than θ_o which depends on the aperture size and the resonant frequency of the transducer by:

$$\theta_o = \sin^{-1}\left(\frac{0.61c}{af_o}\right) \tag{2}$$

where a is the transducer aperture radius and f_o is its resonant frequency [7].

With a single transducer, it is not possible to estimate the azimuth of a target with better resolution than the angular resolution of sonar which is approximately $2\theta_o$. In our system, two identical acoustic transducers a and b with center-to-center separation d are employed to improve the angular resolution (Figure 1). Each transducer can operate both as transmitter and receiver. The

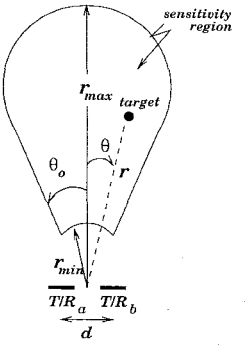

Figure 1: Sensitivity region of an ultrasonic transducer.

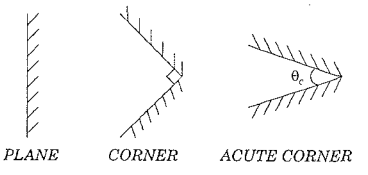

Figure 2: Target primitives modeled and differentiated in this study.

typical shape of the *sensitivity region* of the ultrasonic transducer pair is shown in Figure 1. The extent of this region is in general different for each target type since geometrically or physically different targets, in general, exhibit different reflection properties.

In this study, the target primitives modeled are plane, corner and acute corner whose horizontal cross-sections are illustrated in Figure 2. Since the wavelength of sonar ($\lambda \cong 8.6$ mm at 40.0 kHz) is much larger than the typical roughness of object surfaces encountered in laboratory environments, targets in these environments reflect acoustic beams specularly like a mirror. Hence, while modeling the received signals from these targets, all reflections are considered to be specular which allows transducers both transmitting and receiving to be viewed as a separate transmitter T and virtual receiver R in all cases [9].

Detailed physical reflection models of these target primitives with corresponding echo signal models are provided in [10].

3 Logical Sensing

This study focuses on the development of a logical sensing module that produces evidential information from uncertain and partial information obtained by multiple sonars at different locations. This section deals with the formation of such evidential information using the theory of belief functions. Belief values are generated for each sensor pair and assigned to the detected features: plane, corner and acute corner. These features and their evidential metric obtained from multiple sonars are then fused in Section 4 using the Dempster-Shafer rule of

combination.

Belief function is a mapping from a class of sets to the interval [0,1] that assigns numerical degrees of support based on evidence [11]. This is a generalization of probabilistic approaches where one is allowed to model ignorance about a given situation. Unlike probability theory, a belief function brings a metric to the intuitive idea that a portion of one's belief can be committed to a set but need not be also committed to its complement. In the target classification problem, ignorance corresponds to not having any information on the type of target that the transducer pair is scanning.

In this study, the model of the far-field behavior of a piston type transducer having a circular aperture is used [8]. Differences in the reflection from a plane, corner and acute corner are determined using evidential approximation of geometrical wave propagation. To differentiate the target primitives, a multisensor system that exploits the differences in signal amplitudes and travel times is implemented and formulated in terms of degrees of belief. This logical sensor model of sonar perception is novel in the sense that it models the uncertainties associated with the target type, its range and azimuth as detected by each sensor pair. The uncertainty in the measurements of each sonar pair is represented by a belief function having *feature*, r and θ as focal elements and degrees of belief $b(.)$ assigned to them:

$$BF = \{feature, r, \theta\ ; b(feature), b(r), b(\theta)\} \tag{3}$$

3.1 Feature Fusion from Multiple Sonars

Logical sensing of target primitives is accomplished through a metric as degrees of belief assigned to plane, corner and acute corner according to the amplitude and TOF characteristics of the signals received from these target primitives. The differentiation algorithm is basically an extension of the algorithm in [7] and is detailed in [10]. Here, we focus on the assignment of beliefs to each feature and the feature fusion process:

$$b(p) = (1 - I_4) I_1 \frac{[A_{aa}(\theta) - A_{ab}(\theta)][A_{bb}(\theta) - A_{ab}(\theta)]}{\max[A_{aa}(\theta) - A_{ab}(\theta)] \max[A_{bb}(\theta) - A_{ab}(\theta)]} \tag{4}$$

$$b(c) = (1 - I_4) \frac{I_2[A_{ab}(\theta) - A_{aa}(\theta)] + I_3[A_{ab}(\theta) - A_{bb}(\theta)]}{I_2 \max[A_{ab}(\theta) - A_{aa}(\theta)] + I_3 \max[A_{ab}(\theta) - A_{bb}(\theta)]} \tag{5}$$

if $I_2 \neq 0$ or $I_3 \neq 0$

else 0

$$b(ac) = I_4 \frac{[t_{aa}(\theta) - t_{ab}(\theta)][t_{bb}(\theta) - t_{ab}(\theta)]}{\max\{[t_{aa}(\theta) - t_{ab}(\theta)][t_{bb}(\theta) - t_{ab}(\theta)]\}} \tag{6}$$

where $A_{ab}(\theta)$ denotes maximum value of $A_{ab}(r, \theta, d, t)$ which is the signal transmitted by transmitter b and received by receiver a, and $t_{ab}(\theta)$ denotes TOF extracted from $A_{ab}(r, \theta, d, t)$ at angle θ by thresholding. Definitions of $A_{aa}(\theta)$ and $A_{bb}(\theta)$ are similar. I_1, I_2, I_3 and I_4 are the indicators of the conditions given below:

$$I_1 = \begin{cases} 1 & \text{if } [A_{aa}(\theta) - A_{ab}(\theta)] > \sigma_A \text{ and } [A_{bb}(\theta) - A_{ab}(\theta)] > \sigma_A \\ 0 & \text{otherwise} \end{cases} \tag{7}$$

$$I_2 = \begin{cases} 1 & \text{if } [A_{ab}(\theta) - A_{aa}(\theta)] > \sigma_A \\ 0 & \text{otherwise} \end{cases} \tag{8}$$

$$I_3 = \begin{cases} 1 & \text{if } [A_{ab}(\theta) - A_{aa}(\theta)] > \sigma_A \\ 0 & \text{otherwise} \end{cases} \tag{9}$$

$$I_4 = \begin{cases} 1 & \text{if } [t_{aa}(\theta) - t_{ab}(\theta)] > \sigma_t \text{ and } [t_{bb}(\theta) - t_{ab}(\theta)] > \sigma_t \\ 0 & \text{otherwise} \end{cases} \tag{10}$$

Remaining belief is assigned to an unknown target type, representing ignorance, as:

$$b(u) = 1 - [b(p) + b(c) + b(ac)] \tag{11}$$

According to the Dempster-Shafer rule of combination [11], belief values obtained from two sonar pairs are considered as independent sources of evidence (Table 1):

$$BF_1 = \left\{f_i, b(f_i)\right\}_{i=1}^{4} = \{p, c, ac, u; b(p), b(c), b(ac), b(u)\} \tag{12}$$

$$BF_2 = \left\{g_j, b(g_j)\right\}_{j=1}^{4} = \{p, c, ac, u; b(p), b(c), b(ac), b(u)\} \tag{13}$$

Consensus is obtained as the orthogonal sum:

$$\begin{aligned} BF &= BF_1 \oplus BF_2 \\ &= \left\{h_k, b(h_k)\right\}_{k=1}^{4} = \{p, c, ac, u; b_C(p), b_C(c), b_C(ac), b_C(u)\} \end{aligned} \tag{14}$$

which is both associative and commutative. The sequential combination of multiple bodies of evidence can be obtained for n sensor pairs as:

$$BF = (((BF_1 \oplus BF_2) \oplus BF_3) \ldots \oplus BF_n) \tag{15}$$

Using the Dempster-Shafer rule of combination:

$$b(h_k) = \frac{\sum\sum_{h_k = f_i \cap g_j} b(f_i) b(g_j)}{1 - \sum\sum_{h_k = f_i \cap g_j = \emptyset} b(f_i) b(g_j)} \tag{16}$$

where $\sum\sum_{h_k = f_i \cap g_j = \emptyset} b(f_i) b(g_j)$ is a measure of conflict. The consensus belief function representing the feature fusion process has the metrics

$$b(p) = \frac{b_1(p)b_2(p) + b_1(p)b_2(u) + b_1(u)b_2(p)}{1 - \text{conflict}} \tag{17}$$

$$b(c) = \frac{b_1(c)b_2(c) + b_1(c)b_2(u) + b_1(u)b_2(c)}{1 - \text{conflict}} \tag{18}$$

$$b(ac) = \frac{b_1(ac)b_2(ac) + b_1(ac)b_2(u) + b_1(u)b_2(ac)}{1 - \text{conflict}} \tag{19}$$

$$b(u) = \frac{b_1(u)b_2(u)}{1 - \text{conflict}} \tag{20}$$

In the above equations, the term "conflict" represents the disagreement in the consensus of two logical sensing units, thus representing the degree of mismatch in the fusion of features perceived at two different sonar sites. The metric evaluating conflict is expressed as:

$$\begin{aligned} \text{conflict} = {} & b_1(p)b_2(c) + b_1(c)b_2(p) + b_1(c)b_2(ac) \\ & + b_1(ac)b_2(c) + b_1(ac)b_2(p) + b_1(p)b_2(ac) \end{aligned} \tag{21}$$

The beliefs are then rescaled after discounting this conflict and may be used in further data fusion processes.

Table 1: Target differentiation by Dempster-Shafer rule of combination.

BF_1 / BF_2	plane $b_1(p)$	corner $b_1(c)$	acute corner $b_1(ac)$	unknown $b_1(u)$
plane $b_2(p)$	plane $b_1(p)b_2(p)$	$\emptyset$ $b_1(c)b_2(p)$	$\emptyset$ $b_1(ac)b_2(p)$	plane $b_1(u)b_2(p)$
corner $b_2(c)$	$\emptyset$ $b_1(p)b_2(c)$	corner $b_1(c)b_2(c)$	$\emptyset$ $b_1(ac)b_2(c)$	corner $b_1(u)b_2(c)$
acute corner $b_2(ac)$	$\emptyset$ $b_1(p)b_2(ac)$	$\emptyset$ $b_1(c)b_2(ac)$	acute corner $b_1(ac)b_2(ac)$	acute corner $b_1(u)b_2(ac)$
unknown $b_2(u)$	plane $b_1(p)b_2(u)$	corner $b_1(c)b_2(u)$	acute corner $b_1(ac)b_2(u)$	unknown $b_1(u)b_2(u)$

4 Simulation Results

4.1 Feature Fusion for Plane-Corner Identification

In the simulations, it is assumed that a decision-making unit consisting of a pair of sensors is available with separation $d = 24.0$ cm, mounted on a stepper motor with step size 0.9^o. Signals are simulated according to the models presented in the Appendix for the Panasonic transducer which has a resonant frequency of $f_o = 40$ kHz and $\theta_o = 54^o$. Temporally and spatially uncorrelated zero-mean additive Gaussian noise of standard deviation σ_A is added to the echo signals. At each step of the motor, a pulse is transmitted, four TOF and four amplitude measurements are recorded. The unit scans the mobile robot laboratory area which is a 1.38m×1.15m rectangular room for $-180^o \leq \phi \leq 180^o$ in order to detect corners and planar walls.

The results of the belief assignment process for a single transducer pair located at the center of the room are given in Figure 3. In this figure, $b(p)$ clearly shows that "plane" feature is recognized with high beliefs at right angles around 0^o, -90^o, $+90^o$, $\pm 180^o$ and with highest beliefs in range since these features lie at closest proximity to the sonar. For larger inclination angles, these four planes are confused with corner since the tails of the amplitude characteristics of a plane and corner are similar. The belief $b(c)$ shows that the four corners of the room are identified with highest belief values around $\pm 45^o$ and $\pm 135^o$. The belief chop in the middle of each corner belief curve reflects a pin-type rise in uncertainty at these locations. This is due to the amplitude characteristics of the corner. At $+\varepsilon$, $-\varepsilon$ degrees to the left or to the right of this line, higher beliefs are generated in the recognition of a corner. In the angular interval between the identification of plane and that of corner in $b(u)$, there exists a region of high uncertainty that corresponds to no data acquisition. Here, all the transmitted waveforms bounce off the room boundaries and no return signal is available, thus $b(r) = b(\theta) = 0$.

Simulations we performed further evolved in working with three identical transducer pairs located at different positions in the 1.38m×1.15m rectangular room and their decisions are combined so as to perform the feature fusion by employing the Dempster-Shafer rule of combination.

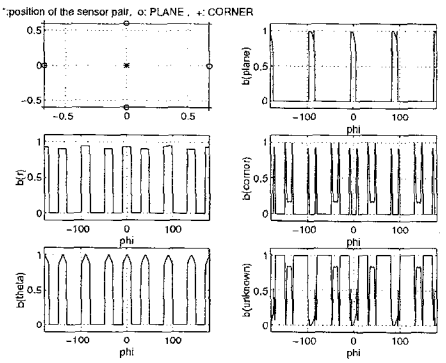

Figure 3: Belief assignment with information from a single transducer pair.

The locations of these transducer pairs are $(0.0, 0.0)$, $(-0.21, 0.17)$ and $(0.35, 0.29)$ in meters where the origin is taken as the center of the room. All transducer pairs are assumed to rotate on stepper motors with step size 0.9^o. These transducer pairs scan the room for $0^o \leq \phi \leq 360^o$. At each step, transducer pairs collect data from the target at the same step angle ϕ, and the decisions of all pairs at this angle are fused. In order to calculate the probabilities of correct classification, misclassification and lack of target identification, data is collected for $0^o \leq \phi \leq 360^o$ three times which corresponds to about 1200 decisions.

The probability of correct classification with the fusion of data from three pairs can be seen in Figure 4. The improvement is around 40% for $\sigma_A < 0.02$ and it is around 20% for $\sigma_A \in [0.02, 0.03]$. For $\sigma_A > 0.03$, there is again an improvement in the probability of correct classification but it is relatively small as compared to the improvements obtained for $\sigma_A < 0.03$. Of course, this is at the increased cost of time to collect more data and do the necessary computations to fuse the data from three pairs of sensors. Dempster-Shafer rule of combination is computationally complex and requires approximately twice the computational effort of Bayesian inference for two or three sensors in a non-parallel implementation [12].

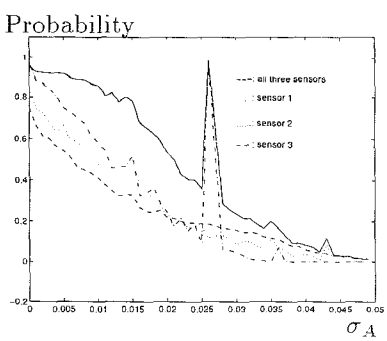

Figure 4: Improvement in the probability of correct classification with data fusion from three sensors.

4.2 Simulation Results with Acute Corner Target Model

In the acute corner simulations, the same sensing configuration is used. An acute corner with wedge angle θ_c is placed in front of the sensor pair at $r = 2$ m as shown in Figure 5. Each time a pulse is transmitted, four TOF and four amplitude measurements are collected. The stepper motor is rotated and the target is scanned for θ from -60^o to 60^o. While obtaining classification results for each case, the transducer pair scans the target from $\theta = -60^o$ to $\theta = 60^o$, 8 times. As a result, the transducer pair makes about 1072 decisions for each pair of σ_t and σ_A values.

For the region in which an acute corner can be reliably differentiated with the classification algorithm ($\theta \in [-20^o, 20^o]$), the results of belief assignments by this transducer pair for three different values of θ_c are obtained and the result for $\theta_c = 60^o$ is given in Figure 6. According to the results obtained, maximum belief value of being an acute corner is one which is obtained at $\theta = 0^o$ for all θ_c values when the system is noiseless. Moreover, the belief of being a plane or a corner is zero for all θ, θ_c and σ_A values in these figures. The values of σ_A used in this analysis are 0.002 and 0.003. Since these beliefs are affected by σ_t, and 0.68 μsec is the minimum value of σ_t obtained at $\sigma_A = 0.002$, 7.61 μsec is its maximum value when $\sigma_A = 0.003$. These values are obtained from the simulations performed to investigate the relationship between σ_t and σ_A which are given in [10]. Although the decrease in the belief of being an acute corner with increasing $|\theta|$ is sharper for larger θ_c, the belief of being an acute corner is greater than the belief of being an unknown target for all θ and σ_A values taking values between 0.8 and 1.0 for $\theta_c = 30^o$, 0.7 and 1.0 for $\theta_c = 45^o$ and 0.6 and 1.0 for $\theta_c = 60^o$ even if $\sigma_A = 0.003$ at which σ_t takes its maximum value in the interval $\sigma_A \in [0, 0.008]$. The limit of this interval $\sigma_A = 0.008$ corresponds to the maximum difference in the echo amplitudes when the maximum value of the echo amplitude is 0.06.

The classification results for the acute corner of $\theta_c = 60^o$ is illustrated in Figure 7. According to the results obtained, the probability of correct classification is higher than both the probability of misclassification and the probability of unknown target up to $\sigma_t = 230$ μsec for $\theta_c = 30^o$, $\sigma_t = 190$ μsec for $\theta_c = 45^o$ and $\sigma_t = 120$ μsec for $\theta_c = 60^o$. Beyond $\sigma_t = 160$ μsec, the probability assigned to unknown target exceeds both the probability of correct classification and misclassification. Moreover, the probability of misclassification becomes greater than the probability of correct classification for $\sigma_t > 300$ μsec.

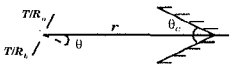

Figure 5: Position of the transducer pair and the acute corner.

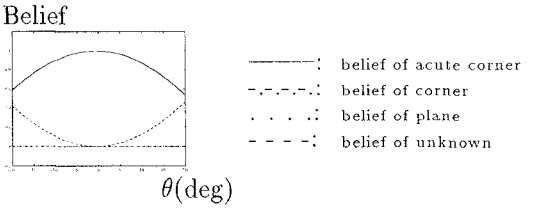

Figure 6: Assignment of beliefs by the sensing unit when an acute corner with $\theta_c = 60^o$ is scanned at $r = 2$ m for $\sigma_A = 0.003$.

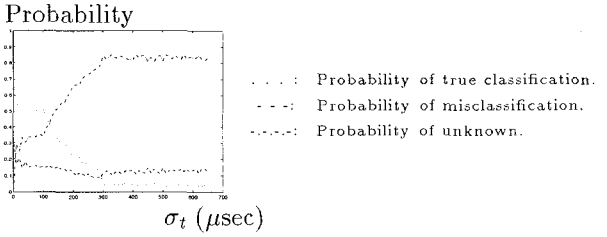

Figure 7: Classification results with a single transducer pair by the first approach when an *acute corner* at $r = 2$ m is scanned with $\theta_c = 60^o$.

5 Experimental Verification

In this study, an experimental set-up is employed to assign belief values to the experimentally obtained TOF and amplitude characteristics of the target primitives, and to test the proposed fusion method for target classification. Panasonic transducers are used which have much wider beamwidth than the commonly used Polaroid transducers. The aperture radius of the Panasonic transducer is $a = 0.65$ cm and its resonant frequency is $f_o = 40$ kHz, therefore $\theta_o \cong 54^o$ for these transducers. Since these transducers are manufactured with distinct characteristics for transmitting and receiving, two pairs of vertically very closely spaced transmitter and receiver, illustrated in Figure 8, are used which approximately behave like the simulated sensor. The horizontal center-to-center separation between the transducers is $d = 24$ cm. This sensing unit is mounted on a small 6 V stepper motor with step size 0.9^o. The motion of the stepper motor is controlled by the parallel port of an IBM-PC 486 and the aid of a microswitch. Data acquisition from the sonars is accomplished by using a DAS-50 A/D card with 12-bit resolution and 1 MHz sampling frequency. Echo signals are processed on an IBM-PC 486 using the C language. Starting at the transmit time, 10,000 samples of each echo signal have been collected and thresholded. The amplitude information is extracted by finding the maximum value of the signal after the threshold value is exceeded.

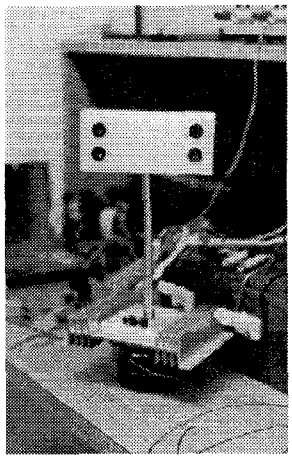

Figure 8: Configuration of the Panasonic transducers in the real system.

Belief assignment results to the TOF and amplitude characteristics of a plane at $r = 50$ cm when scanned with the Panasonic quadruplet are given in Figure 9. In this figure, belief of being a planar type target primitive is greater than zero for $-20^o \leq \theta \leq 20^o$. Belief of being a plane and the belief of being an unknown target oscillate around 0.5 for $|\theta| \leq 10^o$, and the belief of being an unknown target is greater than the belief of a plane outside this region. Moreover, belief of being a corner or an acute corner is zero for all θ values. Estimated range and azimuth values are given in Figure 10. Referring to this figure, maximum range error is 0.5 cm and maximum error in the azimuth estimate is 0.7^o.

Beliefs are assigned to the TOF and amplitude characteristics of a corner at $r = 80$ cm as shown in Figure 11 when scanned with the Panasonic sensing unit. The belief of being a corner is greater than the belief of being an unknown target for all $|\theta| \geq 5^o$ except one point at which the belief of being a plane is one. Belief of plane is zero at all θ values except this point. Estimated range and azimuth values are given in Figure 12. Referring to this figure, maximum range error is 0.3 cm and the maximum error in azimuth estimates is 3.6^o in the region $\theta \in [-5^o, 5^o]$. In Figure 12(c), estimated wedge angle of the acute corner is shown. Although the belief of being an acute corner is around one for $|\theta| \leq 5^o$, estimated wedge angle is around 90^o in this region.

Beliefs assigned to the TOF and amplitude characteristics of an acute corner of $\theta_c = 60^o$ at $r = 40$ cm which is scanned with the same system are given in Figure 13. In this figure, belief of being an acute corner is always greater than the belief of being an unknown target and belief of being a plane or a corner is always zero. Estimated range, azimuth and wedge angle of acute corner are given in Figure 14. Referring to this figure, maximum range error is 2.0 cm, maximum error in azimuth estimates is 3.0^o and maximum error in estimated angle of the acute corner is 4.2^o for the interval $\theta \in [-6^o, 6^o]$.

The results are tested further in an uncluttered rectangular room with specularly reflecting surfaces. A 1.38m×1.15m rectangular room is scanned with three sensing units located at (0.0,0.0), $(-0.21, 0.17)$ and (0.35,0.29) in meters which are the same positions as in the simulation studies. Due to the physical limitations with the hardware, the sensors cannot cover the whole range of ϕ but rotate over the range $0^o \leq \phi \leq 284^o$. The range readings of the transducer pair located at $(-0.21, 0.17)$ are given in Figure 15 as an example.

Beliefs are assigned by the sensors to the TOF and amplitude characteristics reflected from corners and planar walls. The results of belief assignment for each sensor are given in Figure 16. Referring to this figure, with the sensor located at (0.0,0.0), the corners 1 and 3 can be detected correctly but the corner 2 and the walls of the room cannot be differentiated accurately. With the sensor at $(-0.21, 0.17)$, corners 1, 2 and 3 and planes 1 and 2 are detected correctly, but the planes 3 and 4 are detected as corner since differentials in the amplitude of echo which is reflected by planes cannot be detected by this sensor accurately when $r \geq 50$ cm. With the sensor

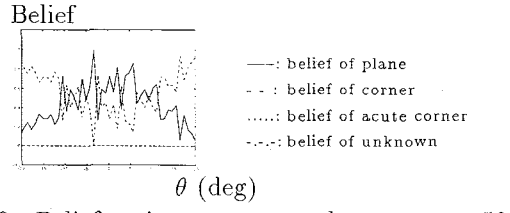

Figure 9: Belief assignment to a plane at $r = 50$ cm scanned with the Panasonic sensing unit.

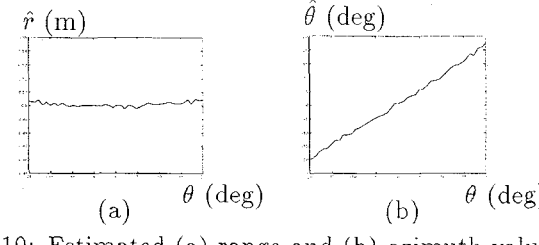

Figure 10: Estimated (a) range and (b) azimuth values of a plane at $r = 50$ cm scanned with the sensing unit.

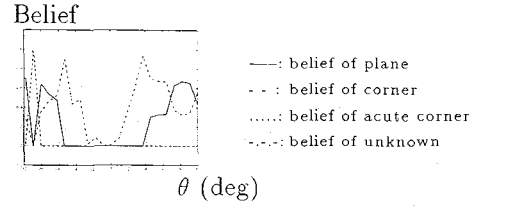

Figure 11: Belief assignment to a corner at $r = 80$ cm scanned with the sensing unit.

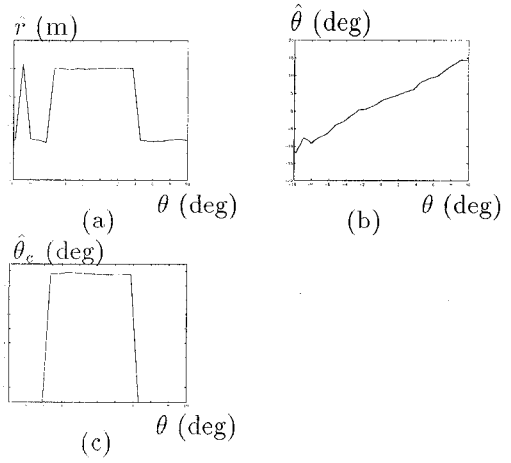

Figure 12: Estimated (a) range (b) azimuth and (c) wedge angle of a corner at $r = 80$ cm scanned with the sensing unit.

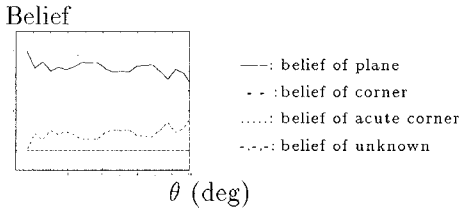

Figure 13: Belief assignment to an acute corner with $\theta_c = 60^o$ at $r = 40$ cm scanned with the sensing unit.

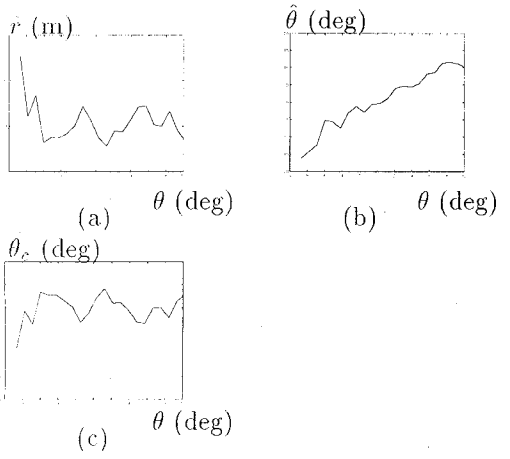

Figure 14: Estimated (a) range (b) azimuth and (c) wedge angle of an acute corner of $\theta_c = 60^o$ at $r = 40$ cm scanned with the sensing unit.

at (0.35,0.29), planes and corners closest to the transducer pair are detected very well but the two furthest planes are detected as corner due to the same reason as explained above.

Pairwise fusion of the beliefs assigned by the sensing unit at each location are given in Figure 17(a)-(c). Referring to this figure, when the beliefs assigned by the sensors at locations (0.0,0.0) and $(-0.21, 0.17)$ are fused, recognition of corners 1 and 3 and plane 2 is improved.

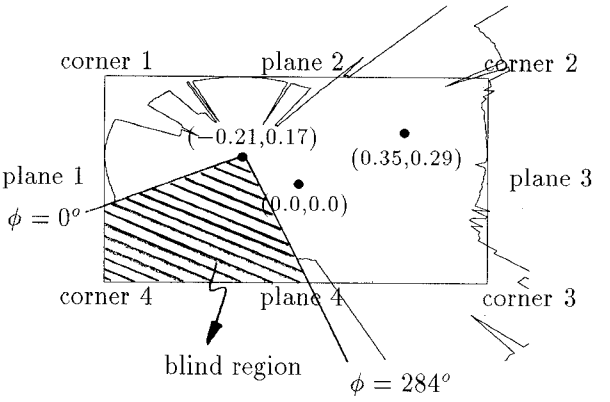

Figure 15: Range readings of the sensor when located at $(-0.21, 0.17)$ in a rectangular room.

When fusion is done for the beliefs assigned by the sensors at (0.0,0.0) and (0.35,0.29), classification of corners 1 and 3 and planes 2 and 3 is improved. However, belief of being a corner at the position of plane 1 increases since both sensors detect plane 1 as corner. Identification of corners 1, 2 and 3 and planes 2 and 3 is improved when the beliefs assigned by the sensors located at $(-0.21, 0.17)$ and (0.35,0.29) are fused. Therefore, the best result for pairwise fusion is obtained when the beliefs assigned by these sensors are fused.

When the beliefs assigned by all three sensors are fused by Dempster-Shafer rule of combination, corners 1 and 3 and plane 2 are detected very well. Corner 2 and plane 3 are detected accurately except for a few values of ϕ. However, plane 1 and plane 4 are detected as corner since the sensors at the locations (0.0,0.0) and (0.35,0.29) detect these planes as corner. Therefore, belief of being a corner is strengthened as can be seen in Figure 17(d).

6 Conclusion

In this study, physical models are used to model reflections from target primitives commonly encountered in mobile robot applications. Target features are generated as being evidentially tied to degrees of belief which are subsequently fused for multiple sonars at distinct geographical sites. Using both TOF and amplitude data the feature fusion process allows more robust differentiation. Belief function approach employed in the differentiation of the target primitives enables the modeling of non-parametric uncertainty. Fusion of feature data from multiple sensors using Dempster-Shafer rule of combination reduces such perception uncertainty but increases the processing time. Nevertheless, it has been experimentally demonstrated that the methodology is suitable for real-time applications when three sensing sites are

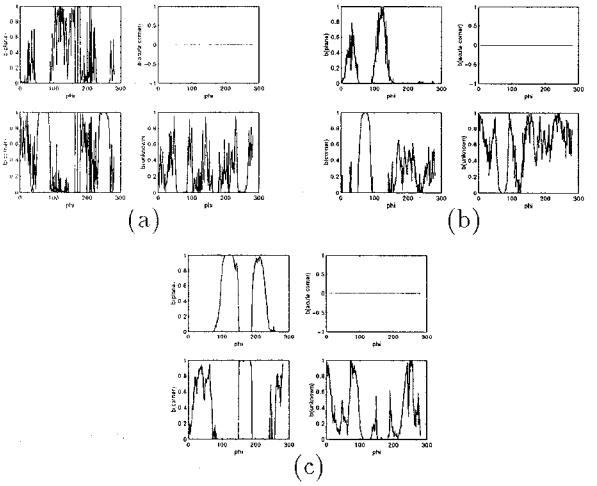

Figure 16: Belief assignment by the sensors located at (a) (0.0,0.0) (b) $(-0.21, 0.17)$ (c) (0.35,0.29).

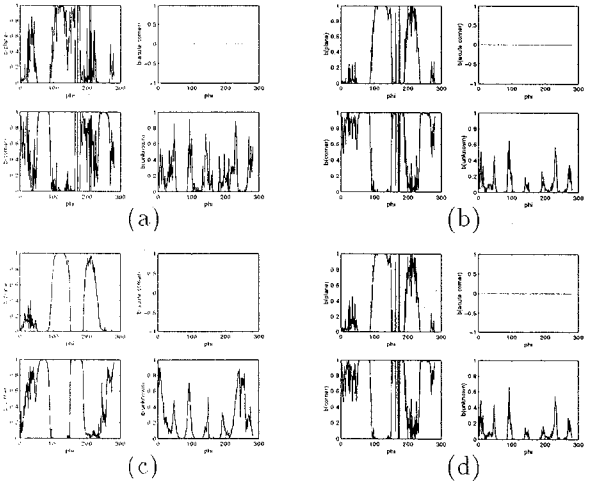

Figure 17: Pairwise fused beliefs for the sensors located at (a) (0.0,0.0) and $(-0.21, 0.17)$, (b) (0.0,0.0) and (0.35,0.29), (c) $(-0.21, 0.17)$ and (0.35,0.29). (d) Results when the decision of all three pairs are fused.

used. The results have ground for application in mobile robotics where multiple sensing agents or robots are employed to survey an unknown environment composed of primitive target types. As for future work, the proposed fusion method can be extended to include physically different sensors such as infrared and laser systems for target identification, localization and tracking applications. The work can be further generalized to three-dimensional targets.

Coordination of the sensing agents and strategic target recognition while either or both the sensors and the targets are in motion is another possible direction for future research.

References

[1] R. Kuc and B. V. Viard, "A physically-based navigation strategy for sonar-guided vehicles," *The International Journal of Robotics Research*, vol. 10, pp. 75–87, April 1991.

[2] J. L. Crowley, "Navigation for an intelligent mobile robot," *IEEE Transactions on Robotics and Automation*, vol. RA-1, pp. 31–41, March 1985.

[3] J. J. Leonard and H. F. Durrant-Whyte, "Mobile robot localization by tracking geometric beacons," *IEEE Transactions on Robotics and Automation*, vol. 7, pp. 376–382, 1991.

[4] R. Kuc, "Three-dimensional tracking using qualitative bionic sonar," *Robotics and Autonomous Systems*, vol. 11, pp. 213–219, 1993.

[5] J. Borenstein and Y. Koren, "Obstacle avoidance with ultrasonic sensors," *IEEE Transactions on Robotics and Automation*, vol. RA-4, pp. 213–218, April 1988.

[6] C. Biber, S. Ellin, E. Sheck and J. Stempeck, "The Polaroid ultrasonic ranging system," in *Proceedings 67'th Audio Engineering Society Convention*, 1990. Reprinted in Polaroid Ultrasonic Ranging System Handbook.

[7] B. Barshan and R. Kuc, "Differentiating sonar reflections from corners and planes by employing an intelligent sensor," *IEEE Transactions on Pattern Analysis and Machine Intelligence*, vol. 12, pp. 560–569, June 1990.

[8] J. Zemanek, "Beam behaviour within the nearfield of a vibrating piston," *The Journal of the Acoustical Society of America*, vol. 49, pp. 181–191, January 1971.

[9] R. Kuc and M. W. Siegel, "Physically-based simulation model for acoustic sensor robot navigation," *IEEE Transactions on Pattern Analysis and Machine Intelligence*, vol. PAMI-9, pp. 766–778, November 1987.

[10] B. Ayrulu. *Classification of Target Primitives with Sonar using two Non-Parametric Data Fusion Methods.* Master's thesis, Bilkent University, Ankara, Turkey, July 1996.

[11] G. Shafer. *A Mathematical Theory of Evidence.* Princeton:Princeton University Press, 1976.

[12] D. L. Hall. *Mathematical Techniques in Multisensor Data Fusion.* Artech House, Norwood, MA, 1992.